A Regionally Enhanced Multi-Phase Segmentation Technique for Damaged Surfaces

Michael O'Byrne

Department of Civil, Structural and Environmental Engineering, Trinity College Dublin, Dublin, Ireland

Franck Schoefs

LUNAM Université, Université de Nantes-Ecole Centrale de Nantes, CNRS, GeM, Institute for Research in Civil and Mechanical Engineering, University of Nantes, Nantes, France; IXEAD/CAPACITES Society, Nantes, France

Vikram Pakrashi*

Department of Civil and Environmental Engineering, University College Cork, Cork, Ireland.

&

Bidisha Ghosh

Department of Civil, Structural and Environmental Engineering, Trinity College Dublin, Dublin, Ireland

Abstract: Imaging based damage detection techniques are increasingly being utilized alongside traditional visual inspection methods to provide owners/operators of infrastructure with an efficient source of quantitative information for ensuring their continued safe and economic operation. However, there exists scope for significant development of improved damage detection algorithms that can characterise features of interest in challenging scenes with credibility. This paper presents a new Regionally Enhanced Multi-Phase Segmentation (REMPS) technique that is designed to detect a broad range of damage forms on the surface of civil infrastructure. The technique is successfully applied to a corroding infrastructure component in a harbour facility. REMPS integrates spatial and pixel relationships to identify, classify, and quantify the area of damaged regions to a high degree of accuracy. The image of interest is pre-processed through a contrast enhancement and colour reduction scheme. Features in the image are then identified using a Sobel edge detector, followed by subsequent classification using a clustering based filtering technique. Finally, Support Vector Machines (SVM) are used to classify pixels which are locally supplemented onto damaged regions to improve their size and shape characteristics. The performance of REMPS in different colour spaces is investigated for best detection on the basis of Receiver Operating Characteristics (ROC) curves. The superiority of REMPS over existing segmentation approaches is demonstrated, in particular when considering High Dynamic Range (HDR) imagery. It is shown that REMPS easily extends beyond the application presented and may be considered an effective and versatile standalone segmentation technique.

* To whom correspondence should be addressed. E-mail: *V.Pakrashi@ucc.ie*.

Keywords: Image Processing, High Dynamic Range (HDR), Receiver Operating Characteristics (ROC), Corrosion, Infrastructure Maintenance Management, Support Vector Machines (SVM).

1 INTRODUCTION

Increasingly exorbitant costs associated with maintaining networks of ageing and deteriorating structures has led to a greater focus on adopting smarter inspection strategies. Regular inspections of the condition of structures are vital to ensure that they remain safe and serviceable. Non-Destructive Techniques (NDT) often provide the only method of obtaining information about the health condition of a structure. This information can be fed into an Infrastructure Management System (IMS), which can help the decision makers to make more effective and informed judgments when allocating resources towards the correction of deficiencies and when choosing an appropriate future course of action. This aspect has attracted a growing interest in recent years as the importance of life cycle optimisation and the related financial benefits continue to be recognised (Sarma and Adeli, 1998; Sirca Jr and Adeli, 2005; Schoefs et al., 2009). For a well calibrated IMS, it is important that the input information is accurate and comprehensive. This requires selecting the most suitable NDT technique, which for a given application is not always readily apparent as a measure of the onsite performance of an NDT technique remains a pertinent question in the majority of cases (Schoefs et al., 2012a). The best NDT method will largely depend on the damage to be detected and will require an in-depth knowledge of the advantages and limitations associated with each option.

There exist a broad range of NDT techniques available. NDT techniques may be partitioned into two categories: non-visual and visual based techniques. Among the non-visual NDT techniques are electromagnetic methods, which include magnetic particle (Groves and Connell, 1985), eddy currents (Yusa et al., 2006) and magnetic flux leakage techniques (Butcher *et al*, 2013). These techniques provide information about surface and near-surface defects and about the effectiveness of cathodic protection systems for metallic structures. Ultrasonic (Iyer *et al*., 2005) and radiographic methods (Correa et al., 2009) can be applied to a wide range of materials and offer capability to detect both external and internal defects. Acoustic Emission (Sohn et al., 2008) methods can be used to monitor the progression of damage and estimate the corrosion in reinforced concrete structures. Finally, there has been growing interest in vibration based techniques such as (Osornio-Rios *et al*, 2012). Visual based techniques offer a good way of detecting anomalies such as corrosion, impact damage and surface-breaking defects. Visual based techniques include image based detection techniques which have applications in the detection of concrete cracks (Nishikawa et al., 2012), object identification in construction sites (Chi and Caldas, 2011), road defect detection from textural pattern recognition (Cord and Chambon, 2012) and assessment of underground pipes (Sinha et al., 2003; Iyer and Sinha, 2006). There are several specialist visual techniques such as remote visual inspection (Nugent and

Pellegrino, 1991) and laser based scanners (Park et al., 2007), yet the most common visual based approach is standard visual inspections carried out by trained engineers.

Many structures are assessed using a conventional regime of visual inspections, performed by trained inspectors/engineers. These inspections cover a range of detail, from a cursory check for gross defects, to a close examination of all surfaces, including the use of special equipment if necessary. The damage is usually qualitatively described and archived by the inspector. An attempt to quantify the severity of the damage is generally made through the use of a numerical scale which typically ranges over a limited number of categories (e.g. 5 levels), leading to a significantly varied degree of uncertainty and vagueness. Moreover, the categories are usually fixed for all types of structures (national or transnational recommendations, owner experience, etc.) based on the pathology of a material even if in some cases the risk analysis calls for a more detailed classification: it leads to errors when classifying critical components or structures. Additionally, whilst numerical scales are helpful for relative ranking and prioritising, they are not easily integrated into future quantitative analyses or experiments and repair options as this level is usually based on qualitative comments based on personal expertise. The quality of visual inspections largely depends on the ability of the inspectors to observe and objectively record details of defects. The approach is prone to considerations such as operator boredom, lapses in concentration, subjectivity, and fatigue, which contribute to the variability and reduced accuracy of visual inspections (Agin, 1980; Komorowski and Forsyth, 2000; Estes & Frangopol, 2003). Visual inspections almost always capture photographs to include in the inspection report to corroborate the inspector's comments; however, these photographs are rarely exploited to their fullest potential in either a qualitative or a quantitative fashion. Moreover, despite the creation of an image archive having an established role in an infrastructure maintenance management framework, it has no agreed protocol of collection and subsequent interpretation (Phares et al., 2004). Adopting an effective image based damage detection approach can provide accurate quantitative information to offset the inherent limitations of conventional visual inspection techniques and increase reliability.

Image based damage detection involves two stages; image acquisition and image analysis. The image acquisition stage uses inexpensive and readily available equipment (i.e. a standard digital camera), and does not require the inspector to undertake extensive training. Furthermore, advances in camera technology mean that rich detailed imagery of damaged components can be acquired. While such rich and high-resolution imagery is advantageous, it can lead to increased processing time for many tasks in the image analysis stage. This is especially pertinent in cases where large batches must be processed. Thus, the image analysis stage should employ powerful yet efficient damage detection algorithms. The aim of the image analysis stage is to locate and quantify the area occupied by visible mechanical damage (typically larger than 10^{-4} m^2) on the surface of infrastructural elements with minimal human supervision. Physical properties of the identified damage, such as the size and shape characteristics, may be easily extracted with knowledge of a real world scale. The quantitative nature

of the data obtained from image analysis is important and naturally lends itself to numerous applications. It is helpful for developing new damage models, or strengthening existing ones, which are used to forecast the rate of propagation of damage as the structure continues to operate.

Damage detection algorithms may consist of image segmentation followed by subsequent classification of the segmented regions, such as (Sinha and Fieguth, 2006). Ideally, the segmentation methodology should identify and accurately define all regions of interest in an image whilst minimizing the inclusion of extraneous regions. In reality, perfect segmentation is difficult to achieve given the inherent chromatic and luminous complexities encountered in natural scenes. Segmentation algorithms use either colour information, texture information, or a combination of both, to isolate similar regions in an image. The effectiveness of colour based segmentation algorithms and texture based segmentation algorithms will vary according to the surface and damage type under consideration as certain damages are more separable from the undamaged surface based on either their colour or texture attributes. The main forms of surface damage encountered on ageing infrastructural elements (corrosion, leaching, etc.) are often characterised to a greater extent by the change in colour from the undamaged surface than a change in texture. With this in mind, the existing texture based segmentation methods for isolating damaged surfaces in the field of NDT such as O'Byrne et al, (2013), can be classified as suitable for specific applications where the damaged regions have a noticeable different texture than the surroundings. Additionally, colour based segmentation algorithms typically have a superior computational efficiency over texture based algorithms given that texture must be calculated by considering a collection of neighbouring pixels around each pixel while colour based segmentation techniques typically need only consider each pixel intensity value independently. Colour based segmentation algorithms may be grouped into four major categories: thresholding, edge detection using gradient information, region growing, and hybrid methods (Abdel-Qader et al., 2008). Existing literature contains a variety of these segmentation methods applied in the domain of NDT. Many of these methods are designed for a particular application such as the detection of weld defects (Alaknanda et al., 2009; Vilar et al., 2009; Yazid et al., 2011; Kasban et al. 2011) or pipe deterioration (Peska, 2001; Liu et al 2012), and/or for particular image sources such as optical (Yazid et al., 2011), thermal (Abdel-Qader et al., 2008; Liu et al 2012; Yishuo and Jer-Wei, 2010; Heriansyah and Abu-Bakar, 2009), ultrasonic (Molero et al., 2012; D'Orazio et al., 2008) and radiography (Alaknanda et al., 2009; Vilar et al., 2009; Yazid et al., 2011; Kasban et al. 2011). As such, while these techniques may be effective for their designated purposes, they are understandably unlikely to perform well when applied to richly detailed, high-resolution optical images of a broad range of surface types and damage forms in complex natural scenes. There exist very few studies that have developed powerful image processing techniques to cater for the detection of damage in challenging circumstances. Thus, the emphasis lies in the development of a new technique that can characterise features of interest in natural scenes with credibility (Lu et al., 1997; Naccari et al., 2005).

This paper presents a novel Regionally Enhanced Multi-Phase Segmentation (REMPS) technique. REMPS is comprised of three phases; identification, classification and enhancement. The first phase generates closed geometries by roughly identifying object boundaries in an image using the Sobel edge detector (Abdou and Pratt, 1979). The classification stage retains regions enclosed by a boundary that represent a damaged zone by employing a clustering based filtering technique. The final phase is dedicated to enhancing the definition of damaged regions by locally supplementing the regions with pixels obtained through SVM classification. SVMs have been used in numerous image segmentation applications (Song and Civco, 2004). Integrating each of these constituent phases in an effective manner creates a powerful and robust detection algorithm. To further improve the detection accuracy of REMPS, High Dynamic Range (HDR) imagery is considered. HDR imagery has previously been proposed as a protocol in the domain of NDT (Ghosh et al., 2010).

The following section details the methodology of the proposed technique as well as providing a brief overview of HDR. Each stage of the methodology is illustrated on an image of a metallic surface suffering from pitting corrosion in coastal conditions. This image is a representative example taken from a large set of images featuring various surfaces and damage forms. Section 3 evaluates the performance of REMPS in various colour spaces (RGB, HSV, and $L^*a^*b^*$) to determine the best segmentation space. REMPS is also compared with several established detection techniques to reveal its noticeable superiority. Section 4 concludes the paper.

2 METHODOLOGY

An image based damage detection algorithm, REMPS, has been proposed in this paper. The algorithm is applied to a Standard Dynamic Range (SDR) image, and the associated HDR image in order to investigate whether adopting a HDR protocol would improve the detection accuracy. This section provides the background to HDR, outlines each of the three phases of the REMPS process, and provides details of the evaluation process used to measure the detection accuracy.

2.1 High Dynamic Range (HDR)

HDR imagery is a set of techniques that allow a greater dynamic range of luminance values between the brightest and darkest regions of an image than standard digital images. SDR images can typically only accommodate a very limited range bracket of the full tonal spectrum in a real world scene. Therefore, a dynamic range bracket would have to be chosen in the knowledge that all luminance values outside the range would not be represented correctly. The broad principle behind HDR imagery is that multiple SDR images of the same scene, each taken at a different exposure, and thus capturing a different range bracket of the tonal spectrum, may be merged to form one HDR image that has a

wider dynamic range (Reinhard et al., 2008). Combining SDR images can be done using various merging algorithms (Naccari et al., 2005; Debevec and Malik, 2008).

The benefits of adopting HDR imagery as an imaging protocol may be observed in Figure 1 which presents three SDR images (an underexposed, a normally exposed and an overexposed image) and the corresponding HDR image. These images depict a 30-year old corroded steel pile in the tidal area in a wharf situated off the French Atlantic Ocean. It may be observed that HDR imagery is particularly useful here since the shiny metallic surface gives rise to a natural high dynamic range. Generally, scenes which have a wide dynamic range due to the presence of bright/shadowy patches or as a result of glossy surfaces are likely to especially benefit from the adoption of HDR as a protocol.

[Figure 1 here]

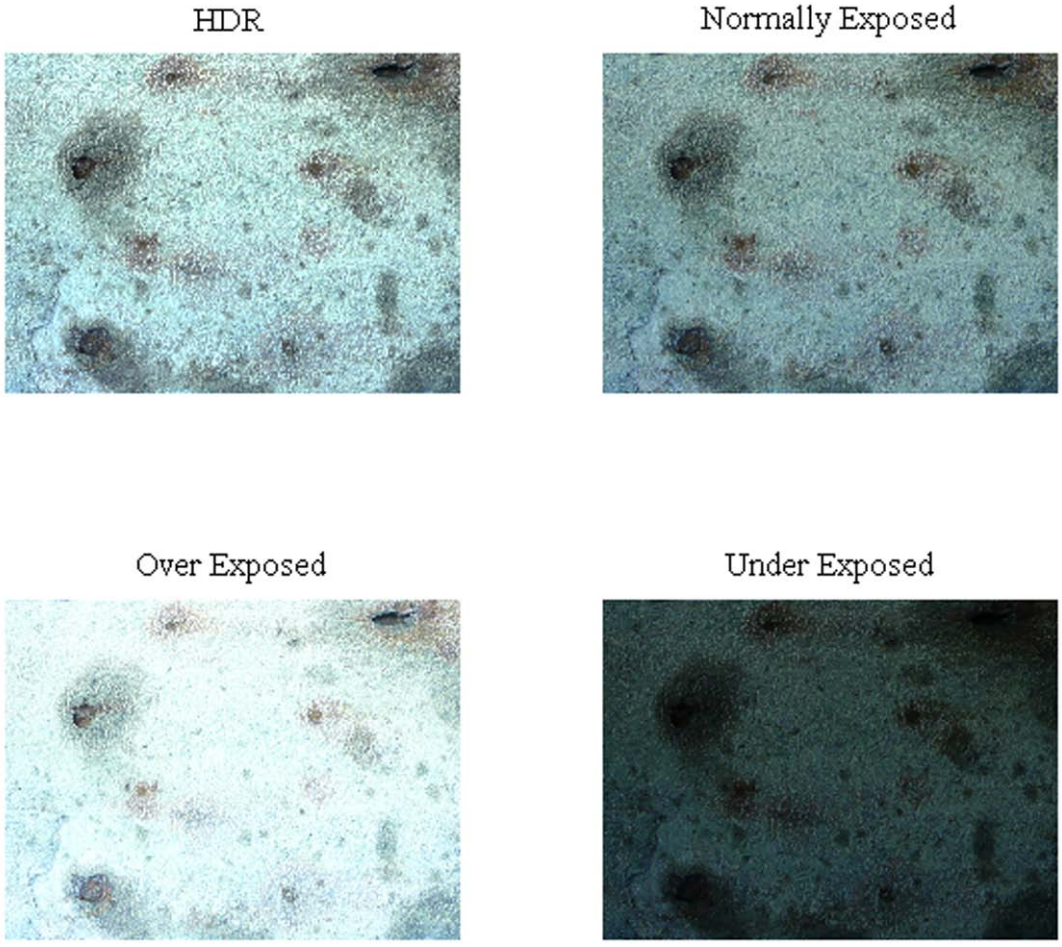

Fig. 1. A High Dynamic Range (HDR) image of corroding steel formed by merging the Normally, Over and Under exposed images together

2.2 Regionally Enhanced Multi-Phase Segmentation (REMPS) technique

The REMPS technique integrates three feature detection methods. A flowchart illustrating the order of the feature detection methods is presented in Figure 2. The first method involves the application of the Sobel edge detector on a modified image in order to form closed geometries corresponding to objects in a scene. Statistical properties are calculated for each of the closed geometries. Statistical based

approaches are popular owing to their computationally inexpensive nature and their robustness (Giralt *et al*, 2013; Li *et al*, 2013). These statistical properties serve as input to a clustering based filtering phase which retains closed geometries that have statistical properties characteristic of damaged regions whilst discarding closed geometries that have statistical properties characteristic of non-damaged regions. SVMs are then used to identify potentially damaged pixels adjacent to these filtered closed geometries in order to improve the definition of the damaged regions. REMPS attempts to utilise the advantages of these three mutually exclusive techniques most effectively. The low complexity of the Sobel edge detector and the clustering based filtering techniques are complimented by the strategic application of the high complexity SVMs. For instance, the robustness and generality of the Sobel edge detector serves as a natural precursor to the closed geometry clustering stage. This clustering stage performs well at classifying the presence of damage, however, it is only after the pixel supplementation stage that the shape and size characteristics of the retained closed geometries are sufficiently realised. Finally, a Receiver Operating Characteristic (ROC) based optimisation framework may be employed to determine the best input parameters. Each stage is discussed in the following sub-sections.

[Figure 2 here]

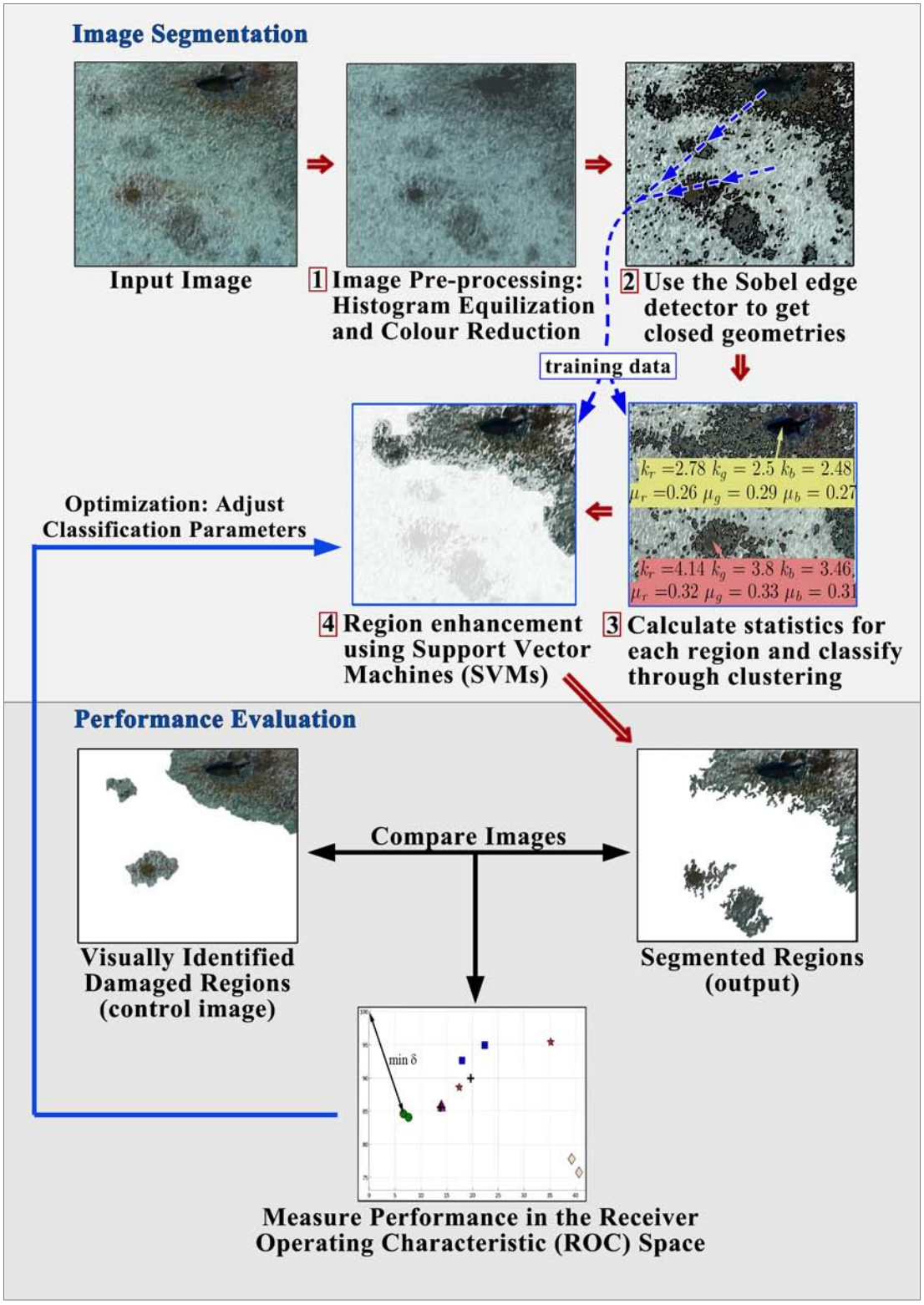

Fig. 1. REMPS Flowchart

2.2.1 Identification

The first stage of the damage identification process involves the creation of a temporary image which undergoes to contrast enhancement and colour reduction operations. These operations help make the boundaries of features of interest in a scene more apparent. This is an important step before the application of the Sobel operator, as often in natural scenes, the transition from damaged to undamaged zones is ambiguous, resulting in an increased likelihood that an edge boundary may be undetected. Contrast is amplified through a process known as Histogram Equalization (HE) (Pizer *et al*., 1987; O'Gorman *et al*, 2008) whereby the intensity values are uniformly spread over the full range of each colour channel in the image [0, 255]. Let A denote an image represented as an M x N x CC matrix of pixel intensity values, where M and N are the row and column lengths and CC is the number of colour channels. For colour images, there are three colour channels (e.g. RGB images are comprised of a Red, Green, and Blue plane). For HE, each colour channel is operated on separately. HE is implemented by firstly calculating the discrete probability, $p_c(i)$, of pixels having intensity i in the c^{th} colour channel of image A :

$$p_c(i) = \frac{n_{i,c}}{n} \qquad \text{for } 0 \le i < L;\ n_{i,c} \le n; \tag{1}$$

where n is the total number of pixels in the image and $n_{i,c}$ is the number of occurrences of pixels with intensity value i in the c^{th} colour channel; L is the total number of intensity levels in the image A (for images defined on a scale of [0, 255], L = 256). L assumes the same value for all colour channels. The Cumulative Distribution Function (CDF), P_c, which provides the accumulated normalized histogram for the c^{th} colour plane can be computed as,

$$P_c(i) = \sum_{\tau \le i} p_c(\tau) \tag{2}$$

With knowledge of the CDF, the general equation for generating the HE image may be written as:

$$heq_c(i) = round\left(\frac{P_c(i) - P_c(i=0)}{(M \times N) - P_c(i=0)} (n_b - 1) \right) n_b \le L \tag{3}$$

where $heq_c(i)$ is the histogram equalized intensity value in the c^{th} colour plane. This equation incorporates colour reduction which quantizes the intensity values in each colour channel into n_b discrete bins. Finally for this preliminary modification stage, a 2D greyscale image, B, of size M x N, is formed by averaging the intensity values from each colour channel as per Equation 4. This equation also includes a scaling term, $\frac{255}{n_b - 1}$, for restoring the image's range from [0, n_b-1] to the original range of [0, 255].

$$\bar{b}(i) = round\left(\frac{255}{n_b - 1} \frac{1}{CC} \sum_{c=1}^{CC} heq_c(i) \right) \tag{4}$$

where $\bar{b}(i)$ is the corrected intensity value in image B . The function of the rounding operator is to ensure that the intensity values in image B remain discrete integers.

A value of 14 was used for n_b for each application of REMPS on the sample images shown throughout this paper. This value was chosen as it was experimentally found to offer a sufficient number of distinct bins and provide suitable grouping of perceptually similar pixels within each bin. The n_b parameter be optimised through a Receiver Operating Characteristic (ROC) based optimisation framework/trial and error approach. Initial detection of features of interest may now be carried by applying an edge detector to the modified image.

The Sobel operator edge detector works by calculating approximations of the first derivatives of an image in horizontal and vertical directions respectively (Abdou and Pratt, 1979). Denoting G_{horz} and G_{vert} as the two masks which give the horizontal and vertical derivative approximations at each point as

$$G_{horz} = \begin{bmatrix} -1 & 0 & +1 \\ -2 & 0 & +2 \\ -1 & 0 & +1 \end{bmatrix} * B \;\; and \;\; G_{vert} = \begin{bmatrix} -1 & -2 & -1 \\ 0 & 0 & 0 \\ +1 & +2 & +1 \end{bmatrix} * B \tag{5}$$

where the asterisk denotes the 2-dimensional convolution operation. A padding with a thickness of one pixel may be applied around the border of image B during the convolution process thereby enabling the computation to be performed at the image extremities. The intensity values in the padding assume the value of the neighbouring pixel in the original image. At each point in the image, the resulting gradient approximations can be combined to give the gradient magnitude, using

$$G = \sqrt{G_{horz}^2 + G_{vert}^2} \tag{6}$$

A large value of G represents a sharp change in image intensity which in turn is indicative of an edge boundary. Since the preliminary histogram equalization and colour reduction steps prevent the occurrence of weak edges, all non-zero values of G may be taken as being representative of an edge. The detected boundaries for the HDR image are shown in Figure 3. The region enclosed by the boundary is denoted by R_j where j is the index of the region (j=1,…,J).

[Figure 3 here]

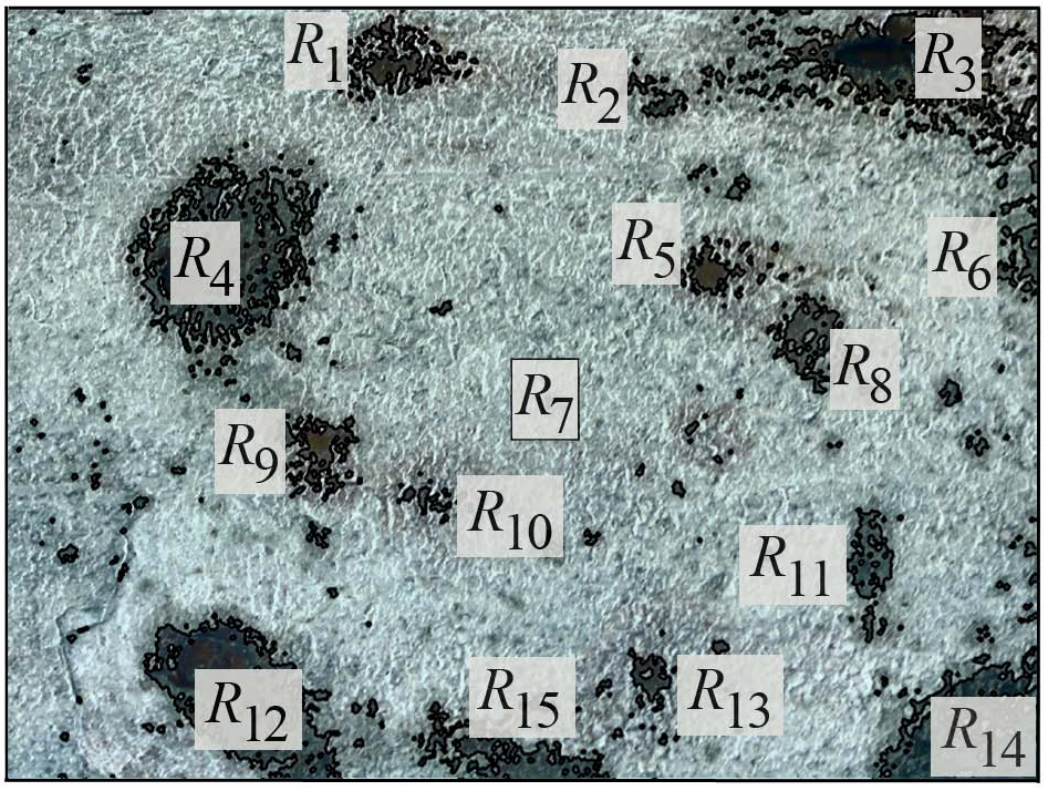

Fig. 3. Detected closed geometries following pre-processing and application of the Sobel operator

It may be observed from Figure 3 that many closed geometries detected by the Sobel operator are of a negligible size which tend to represent spurious regions rather than damaged regions. For computational parsimony and classification accuracy purposes, closed geometries below a certain size are not considered for future analysis. The chosen threshold area can be viewed as the minimum defect size, below which regions are considered to present an insignificant degree of damage. It may be convenient to represent the threshold area as a function of the overall image size. For instance, it could be specified that closed geometries less than 1% of the total image area should be discarded. A priori knowledge of the damage type and its relationship to the decision process (repair, detailed inspection etc.) may be used as a factor in choosing the threshold area. The remaining closed geometries are classified by means of a clustering technique.

2.2.2 Clustering based Filtering

Given a set of closed geometries ($R_j = R_1 , R_2,..., R_J$), the clustering algorithm aims to partition the J observations into two sets $S = \{S_1, S_2\}$ such that the Euclidean distance between the centroid of R_j and the centroid of the set which it is assigned to is minimized. S_1 corresponds to the cluster representing damaged regions while S_2 represents the undamaged cluster.

The centroid of each closed geometry is given by the point $(\mu_1,\mu_2,\mu_3,k_1,k_2,k_3)_j$ where $u_{1\text{-}3}$ is the mean, and $k_{1\text{-}3}$ is the kurtosis, of the pixel distribution for each of the three colour channels within the j^{th} closed geometry. The mean of each colour channel for each region is computed by :

$$\mu_{c,j} = \frac{1}{n_{R_j}}\left(\sum_{t=1}^{n_{R_j}} i_{t,c,j}\right) \qquad \in R_j \tag{7}$$

while the kurtosis is given by:

$$k_{c,j} = \frac{1}{n_{R_j}}\left(\sum_{t=1}^{n_{R_j}} (i_{t,c,j} - \mu_{c,j})^4\right) \qquad \in R_j \tag{8}$$

where $i_{t,c,j}$ denotes the intensity value for the pixel with index t within the jth region for the c^{th} colour channel, while n_{R_j} denotes the total number of pixels in the j^{th} region. The properties of mean and kurtosis were chosen as they were found to sufficiently describe the pixel distribution of each closed geometry. Representing a closed geometry solely based on the mean is susceptible to error as closed geometries with disparate pixel distributions may yield similar values. Introducing kurtosis offsets this issue and creates a more well-rounded description of each closed geometry. Its amplitude independent nature means that it is less effected by variations in contrast levels between images within a batch, ensuring that training data selected in one (or more) image(s) remains applicable to other images in the batch. Furthermore, it was experimentally found to provide a good description of damaged regions. A scatter plot of the mean and kurtosis values for the numbered regions in Figure 3 is illustrated in Figure 4b. The centroid of the j^{th} closed geometry, R_j, is given by $(\mu_1,\mu_2,\mu_3,k_1,k_2,k_3)_j$. The centroids of the damaged and undamaged clusters are obtained from the training data. The training data is comprised of two closed geometries which are representative of a damaged and undamaged zone. These regions must be manually selected. In the illustrated example, the region labelled "R_1" in Figure 3 was used as the damaged training data while the background was chosen as the undamaged region (labelled "R_7"). The cluster centroid for the damaged cluster, S_1, is thus given by the vector $(\mu_1,\mu_2,\mu_3,k_1,k_2,k_3)_1$, while the centroid of the undamaged cluster, S_2, is given by $(\mu_1,\mu_2,\mu_3,k_1,k_2,k_3)_7$.

[Figure 4 here]

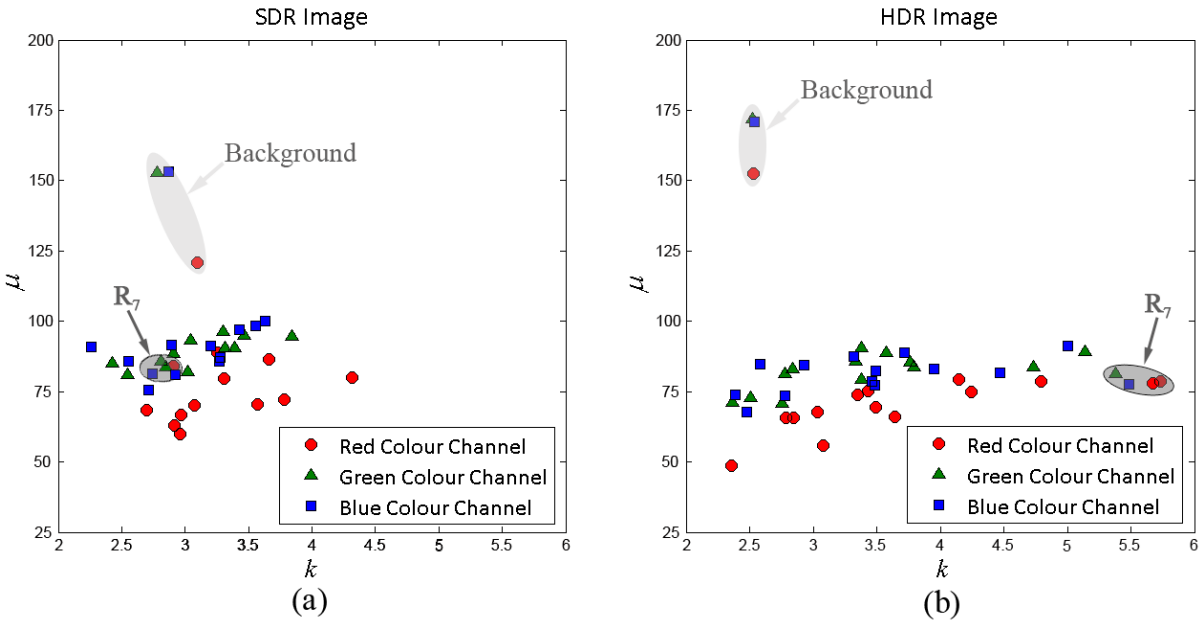

Fig. 4. Scatter plot of mean and kurtosis values for each closed geometry in the (a) SDR and (b) HDR images

Figure 4 illustrates the difference between the range of μ and k values in the SDR and HDR images. It may be observed from the HDR image scatter plot (Figure 4b) that there is a greater degree of separation, according to μ, between the background and the other closed geometries in comparison to the SDR image scatter plot (Figure 4a). Additionally, the scatter points for the HDR image are more dispersed, according to k, which should, in theory, facilitate clustering by reducing the likelihood of ambiguous closed geometries that lie on the decision boundary.

R_j is assigned to the set which minimises the Euclidean distance between the observation centroid and cluster centroid as:

$$R_j \in \begin{cases} S_1, & \text{if } \sum_m \left\| R_{j,m} - R_{damaged,m} \right\|^2 \leq \sum_m \left\| R_{j,m} - R_{undamaged,m} \right\|^2 \\ S_2, & \text{otherwise} \end{cases} \quad (9)$$

where m = 1,2,...,6 denotes the index of the elements in R_j.

Once the closed geometries have been grouped into their respective clusters, it is necessary to enhance their size and shape characteristics.

2.2.3 Enhancement

Following the region based clustering stage, there still exists many damaged pixels around the periphery of the region that remain undetected Performing SVM in the neighbourhood of these regions and then locally supplementing the closed geometries with the SVM pixels produces better

defined features of interest. This is conveyed by comparing the closed geometry R_1 before and after the local application of SVM classified pixels (Fig. 5a and 5b respectively).

Fig. 5. Close-up of R_1, (a) Before local enhancement, and (b) Detected pixels from SVM classification

SVMs are used to classify pixels as being either damaged or undamaged based on the intensity values for each colour channel. SVM is a supervised learning classifier based on statistical learning theory. The linear SVM is used for linearly separable data using a (*f*-1) dimensional hyperplane in *f* dimensional feature space (Vapnik, 1995; Boser et al. 1992; Cortes and Vapnik, 1995; Cristianni and Shawe-Taylor, 2000). This hyperplane is called a maximum-margin hyperplane which ensures maximized distance from the hyperplane to the nearest data points on either side in a transformed space. The linear kernel function is the dot product between the data points and the normal vector to the hyper-plane. The kernel function concept is used to simplify the identification of the hyperplane by transforming the feature space into a high dimensional space. The hyperplane found in the high dimensional feature space corresponds to a decision boundary in the input space.

In SVM the classifier hyperplane is generated based on training datasets. The same damaged and undamaged regions used in the clustering stage are used as the training data. Given a training dataset of l points in the form $\{(u_h, v_h)\}_{h=1}^{l}$ where h denotes the h^{th} vector in the dataset, u_h is a real f-dimensional input vector containing the mean and kurtosis values associated with each region $u_h \in \Re^f$ and v_h is an instance label vector $(v_h \in \{1,-1\}^l)$; for this study, a value of +1 indicates presence of damage and -1 indicated absence of damage. To identify the maximum-margin hyperplane in the feature space, the SVM requires the solution of the following optimization problem:

$$\{w,e\} = \arg\min_{w,b,\xi}\left(\frac{1}{2}w^T w + C\sum_{h=1}^{l}\xi_h\right);\ C>0$$
$$\text{subject to } v_h(w^T\varphi(u_h)+e) \geq 1-\xi_h;\ \ \xi_h \geq 0 \tag{10}$$

The function φ maps the training vectors u_h into a higher dimensional space. The vector *w* is the weight vector which is normal to the hyperplane, *e* is the bias, ξ is the misclassification error and *C* is the cost or penalty parameter related to ξ. The solution to the problem is given by:

$$\min_{\alpha} \left(\frac{1}{2} \sum_{h=1}^{l} \sum_{q=1}^{l} \alpha_h \alpha_q v_h v_{x,y} K(u_h, u_{x,y,c}) - \sum_{h=1}^{l} \alpha_h \right) \tag{11}$$

With Constraints:

$$\begin{aligned} &\sum_{h=1}^{l} \alpha_h v_h = 0 \\ &0 \le \alpha_h \le C, h = 1, ..., l \end{aligned} \tag{12}$$

Where *K* is the kernel function α_h and α_q are the Lagrange multipliers, $v_{x,y}$ is a label vector $(v_{x,y} \in \{1, -1\})$ for the input point $u_{x,y,c}$. The linear kernel has been used here,

$$K(u_h, u_{x,y,c}) = u_h{}^T u_{x,y,c} \tag{13}$$

There is one preselected parameter value for the SVM, namely the cost parameter *C*, which may be optimised in a similar fashion to the n_b parameter from the colour reduction stage using an ROC based optimisation framework/trial and error approach.

The enhancement process firstly examines pixels that are immediately adjacent to each retained region, R_j. A pixel is considered to be adjacent to a region if it shares an edge or corner with any pixel on the periphery of that region. SVM classification is applied to these adjacent pixels utilising their original intensity values ($a_{x,y,c}$) to classify each of these pixels as representing damaged surface or not. Pixels which are classified using SVMs as representing damage become a member of the region, R_j. Pixels in immediate vicinity of the newly identified member pixels of R_j are further subjected to classification using SVMs. This process is repeated until there are no more adjacent damaged pixels that can be added to a region. For computational parsimony, no individual pixel is subjected to classification using SVMs more than once in the entire region enhancement step.

2.3 Performance measures of REMPS

The performance of the REMPS technique is evaluated through the use of performance points in the ROC space. The ROC space allows for a convenient means of characterising and comparing the performance of NDT methods in various conditions (Rouhan and Schoefs, 2003) and has been recently expanded to image detection (Pakrashi *et al*., 2010). For any NDT, the Detection Rate (*DR*) along with the accompanying Misclassification Rate (*MCR*), or alternatively known as Probability of Detection (*PoD*) and Probability of False Alarm (*PFA*) in the field of probability space and decision theory, are determined by comparing the corroded regions detected with a visually segmented image. The visually segmented image is created by a human operator who manually identifies damage in an

image. It acts as the control as it is assumed it shows the true extent of damage. The visually segmented image only needs to be created when it is wished to gauge the performance levels of the technique under scrutiny. The *DR* and *MCR* are represented as a percentage between 0% and 100%. Each (*MCR*,*DR*) pair formed a coordinate in the ROC space. The *DR* and *MCR* are defined as:

$$DR \approx \frac{Card(E)}{n_c} \text{ with } \quad E = \left\{ g \in \Im ; \gamma_g = 1 \right\} \tag{14}$$

$$MCR \approx \frac{Card(F)}{n} \text{ with } \quad F = \left\{ g \in \Im ; \gamma_g = -1 \right\} \tag{15}$$

where *Card(.)* indicates the cardinal of a particular set, $\Im = \{1, \ldots, n\}$. n_c denotes the number of damaged pixels and γ_g is an instance label vector $(\gamma_g \in \{1, -1\})$, where $\gamma_g = 1$ corresponds to correctly identified damaged pixels and $\gamma_g = -1$ corresponds to incorrectly detected pixels and undetected damaged pixels. *F* gathers situations of incorrectly detected pixels and undetected damaged pixels while *E* gathers the correctly detected ones. A box counting approach (O'Byrne et al., 2011) was employed to calculate n_c for each image in each colour space.

There are a few measures for comparing segmentation performance (Hui et al., 2008). In this paper, a measure of the performance is obtained through the use of the α-δ method (Baroth et al., 2011; Schoefs et al., 2012b). This method relies on calculating the angle, α, and the Euclidean distance, δ, between the best performance point, defined as an ideal NDT with 100% detection and 0% misclassification rates and represented in the ROC space with coordinates (0,1) and the considered point to give a measure of the performance of the considered point. As this paper does not deal with risk analysis where the shape to the ROC acts as a key factor, only the delta, δ, parameter is required as a measure of performance. A low value for δ is indicative of a strong performance.

3 EVALUATION OF REMPS

This section presents the results obtained by REMPS when applied to the SDR (normally-exposed) and HDR images of pitting corrosion (Figure 1). The performance is investigated for several colour spaces. These colour spaces are introduced in the first subsection. A comparison of the results for each colour space is provided in the second subsection, while the final subsection compares the performance of REMPS with established detection techniques.

3.1 HSV and *L*a*b* colour spaces

Two additional colour spaces were considered in order to determine whether this could improve the accuracy of detection, namely the HSV and *L*a*b** spaces. HSV (Hue, Saturation, Value) is one of several variations of colour spaces characterised by the factors in the parenthesis. It is often used in

computer vision and image analysis for feature detection or image segmentation as the hue component is believed to be especially useful for separating objects with different colours (Vapnik, 1995). Often, detection algorithms applied to colour images are extensions to algorithms designed for greyscale images whereby each of the three colour channels is separately passed through the same algorithm. It is important, therefore, that the features of interest can be distinguished by the colour dimensions used. Because the red, green and blue components in an RGB image are all correlated with the same amount of light hitting the object, and therefore with each other, image descriptions in terms of these components can make object discrimination difficult. Descriptions in terms of hue-saturation-brightness are often more relevant due to this separation of chromatic and achromatic information. The HDR image of pitting corrosion is shown in the HSV colour space in Figure 6b.

The *L*a*b** colour space also offers some interesting benefits over the RGB space, especially in cases where the colour of damaged zones is perceptually close to the colour of the undamaged surface. The *L*a*b** space consists of a luminosity layer *L**, and chromaticity layers *a** and *b**. The *L** component is similar to the V component HSV space. It closely matches the human perception of lightness. Being able to isolate the lightness layer is helpful for making accurate colour balance corrections which is useful when environmental conditions such as lighting levels cannot be controlled (O'Byrne et al, 2013). The colour information is stored in the *a** and *b** layers. The *a** component indicates where the colour lies on the red-green axis, while the *b** component indicates where the colour lies on the blue-yellow axis. The *L*a*b** space attempts to reflect a uniform change in perceived colour with a corresponding uniform change in the *L**, *a**, and *b** components. The HDR image in the *L*a*b** colour space is shown in Figure 6c.

3.2 Comparison of colour spaces

Different colour spaces encode and numerically represent colour in various ways. Consequently, some colour spaces are more receptive to certain segmentation techniques than others. REMPS is applied to the SDR and HDR images in the RGB, HSV and *L*a*b** colour spaces to explore whether a particular colour space responds well to the proposed technique. The detected regions for the HDR image in each colour space are shown in Figure 6. The performance of REMPS for the SDR and HDR images in each colour space are quantified in Table 1 and the associated performance points are plotted in the ROC space in Figure 7.

[Figure 6 here]

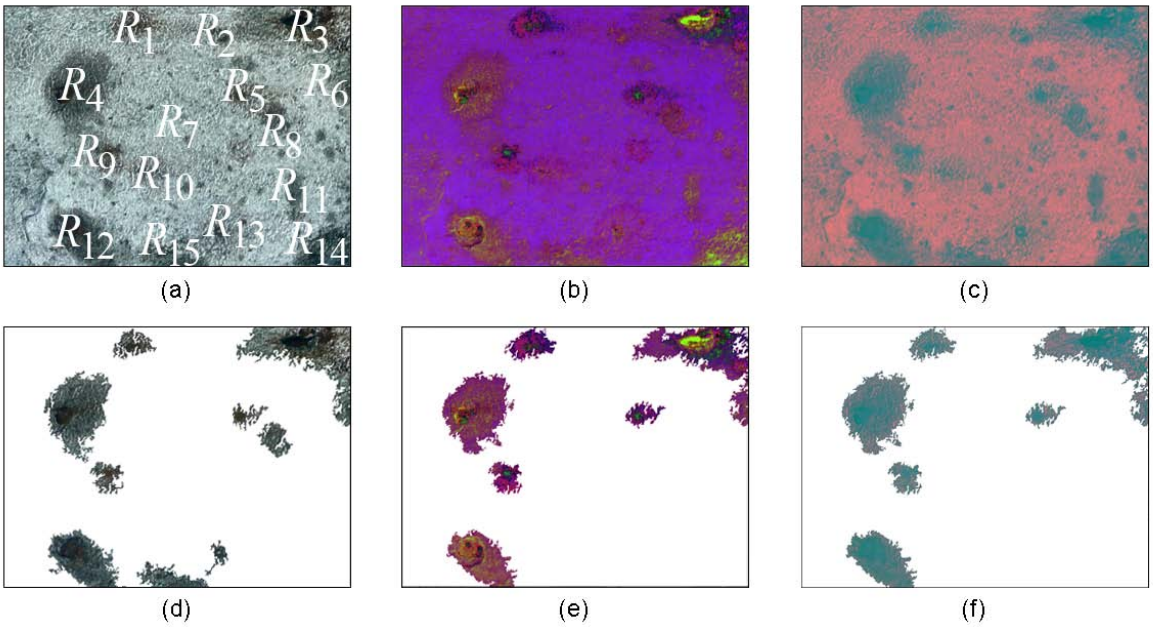

Fig. 6. HDR Image of Pitting Corrosion. (a) Image in RGB space, (b) Image in HSV space, (c) Image in *L*a*b** space, (d) Detected Regions in RGB, (e) Detected Regions in HSV, (f) Detected Regions in *L*a*b**.

Table 1

Detection accuracy for the SDR and HDR image of pitting corrosion for each colour space.

Colour Space	SDR Image			HDR Image		
	DR	MCR	δ	DR	MCR	δ
RGB	84%	8%	0.18	85%	7%	0.17
HSV	85%	7%	0.17	84%	5%	0.17
*L*a*b**	76%	5%	0.24	85%	5%	0.16

[Figure 7 here]

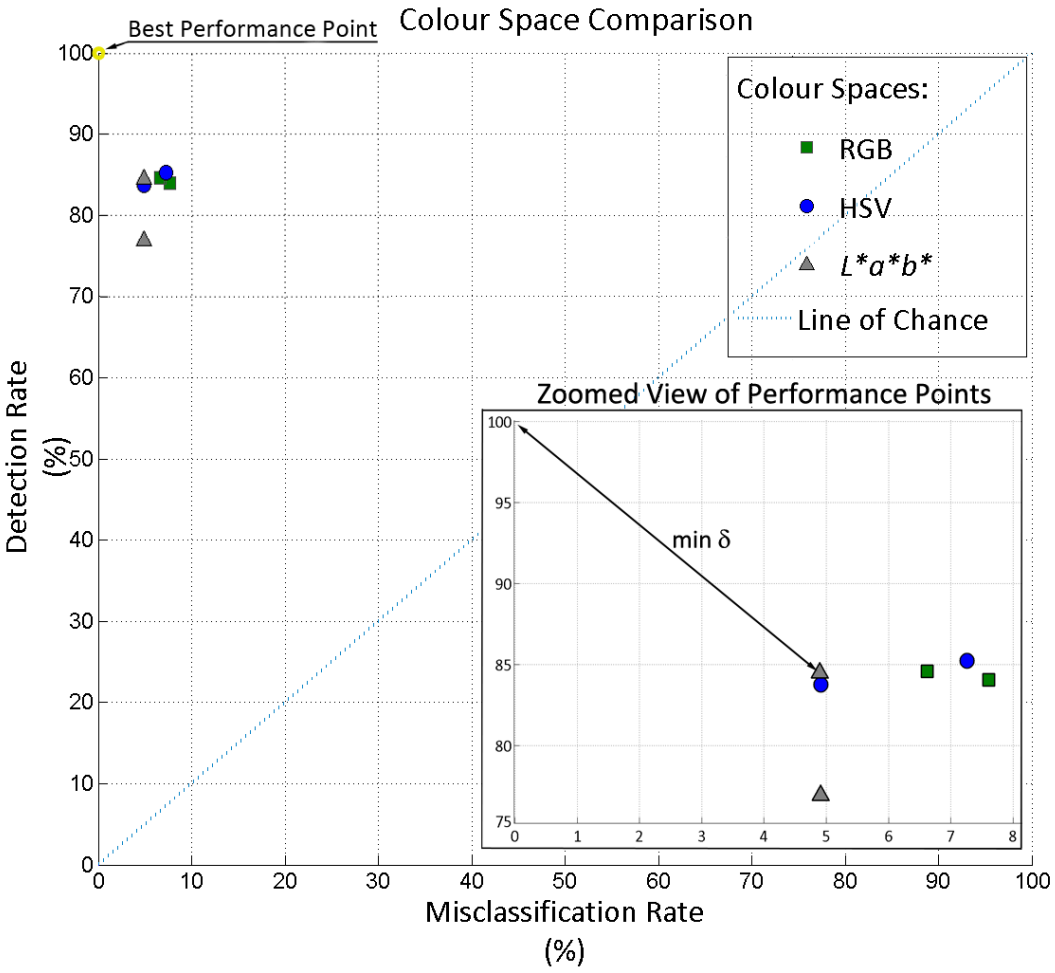

Fig. 7. ROC curves depicting the performance of REMPS algorithm in various colour spaces.

It may be observed from the relatively compact nature of performance points in Figure 7 that the accuracy of REMPS is not heavily reliant on the colour space. Despite this, some interesting findings emerged. The HDR image typically offered a superior performance over the SDR image. Overall, it was the HDR image in the *L*a*b** space that achieved the best performance while, conversely, the SDR image in *L*a*b** was the worst performer by noticeable margin. This suggests that adopting a HDR protocol is especially relevant when operating on images in the *L*a*b** space.

The performance order of the colour spaces might be somewhat expected given the visual appearance of the HDR image in each colour space (Figure 6a-6c). It may be noted that damaged regions in *L*a*b** appear relatively homogenous and are readily discernible against the background. The damaged regions in the HSV colour space on the other hand are composed of several colours making object detection more difficult. The RGB space is slightly more effective than the other spaces at locating the presence of damage while the HSV and *L*a*b** spaces perform well at defining the shape and size of damaged regions.

The success of REMPS is influenced to varying extents by the performance of each phase in a given colour space. While there is a heavy reliance on the ability of the Sobel edge detection phase to

isolate damaged regions, it is the clustering stage which has the greatest influence. This stage determines whether clusters should be retained or discarded so it can have a significant impact on both the misclassification and detection rate. Conversely, the SVM stage has a relatively minor effect on the detection accuracy as it is largely confined to a role as a supplementary tool to enhance already detected regions. Thus, colour spaces that do not respond well to the edge detection stage and particularly the clustering stage are greatly handicapped.

3.3 Comparison with Traditional Colour based Techniques

In this section, REMPS is compared with established detection techniques, such as Otsu's Method (Otsu, 1979), Chan-Vese Method (Chan and Vese, 2001), Delaunay Triangulation (Cheddad et al., 2008), Region Growing (Adams and Bischof, 1994), and Graph-Based Segmentation (Felzenszwalb and Huttenlocher, 2004). The comparison serves to highlight the effectiveness of REMPS in relation to the other segmentation techniques. The regions detected using these techniques on the HDR image are shown in Figure 8, and their respective performances are quantified in Table 2 for both the SDR and HDR images, as well as being graphically illustrated by means of performance points in the ROC space in Figure 9.

The performance of colour based segmentation techniques is affected by whether the technique is contextual or non-contextual. Non-contextual techniques (e.g. thresholding) do not take into account any spatial relationships between pixels in an image, but rather segment pixels at a global level on the basis of some attribute, e.g. colour intensity. Contextual techniques (e.g. REMPS or region growing techniques) on the other hand do consider spatial relationships. If a contextual relationship is an important factor for segmenting a particular image, than non-contextual techniques will have limited success compared to techniques which exploit the contextual relationship. Adopting the $\alpha\delta$ method allowed for an clear comparison between various (*DR,MCR*) pairs. Analysis of the δ parameter in Table 2 reveals that all of the established techniques performed noticeably better when applied to the SDR image rather than the HDR image. In some cases, such as for the Region Growing technique (Figure 8d), the SDR image offered an appreciably improved performance suggesting that the increased local contrast associated with HDR has an adverse effect . This may be observed from the ROC space in Figure 9 which illustrates the relatively separate nature of the two performance points associated with the technique. However, an exception to this trend emerged in the case of REMPS, whereby the performance was slightly enhanced when HDR imagery was considered as an imaging protocol.

The performance levels obtained from each technique varied markedly. The Chan-Vese method (Figure 8b) and Delaunay Triangulation (Figure 8c) performed quite well when applied to the SDR image, whilst Otsu's Method (Figure 8e) performed reasonably well on both the SDR and HDR

images despite its simple and non-contextual nature. The Graph Cutting technique (Figure 8f) on the other hand produced poor results, as demonstrated by the performance points in the ROC space lying closer to the line of chance than the best performance point (Figure 9). Overall, the REMPS achieved the best detection results, especially when performed on the HDR image.

[Figure 8 here]

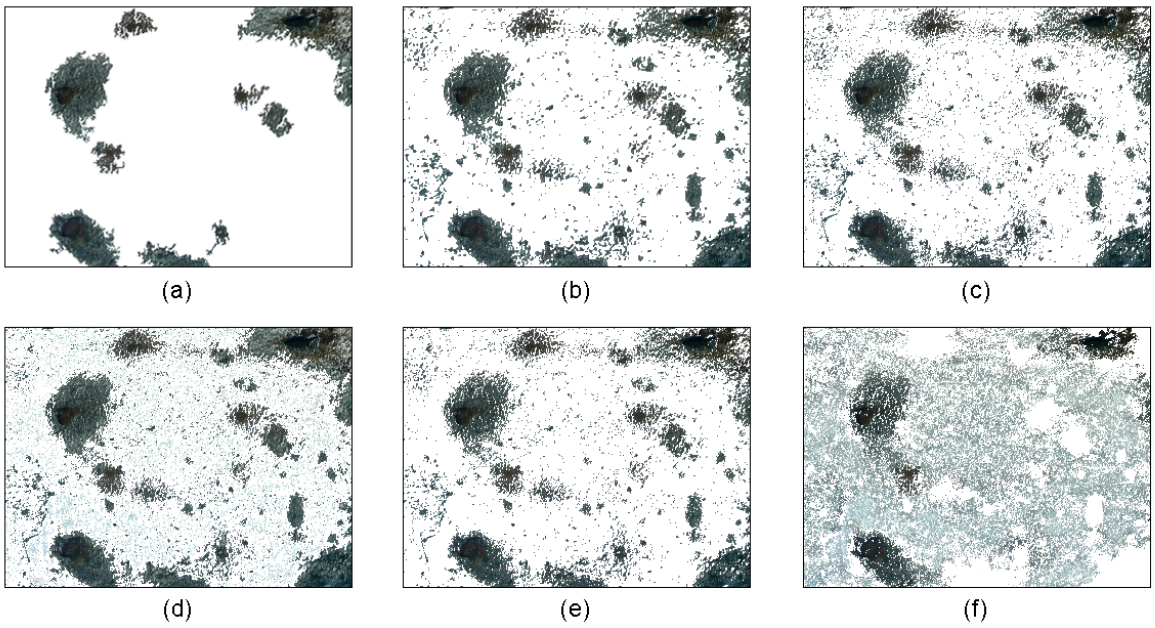

Fig. 8. Detected Regions from: (a) REMPS, (b) Chan-Vese Method, (c) Delaunay Triangulation, (d) Region Growing, (e) Otsu's Method, (f) Graph-Based Segmentation.

Table 2

Comparison of techniques.

Segmentation Technique	Normally Exposed Image			HDR Image		
	DR	MCR	δ	DR	MCR	δ
REMPS	84%	8%	0.18	85%	7%	0.17
Chen-Vese	93%	18%	0.19	95%	22%	0.23
Delaunay Triangulation	86%	14%	0.20	85%	14%	0.20
Region Growing	89%	17%	0.21	95%	35%	0.36
Otsu's Method	86%	14%	0.20	90%	20%	0.22
Graph Cutting	78%	39%	0.45	76%	41%	0.47

[Figure 9 here]

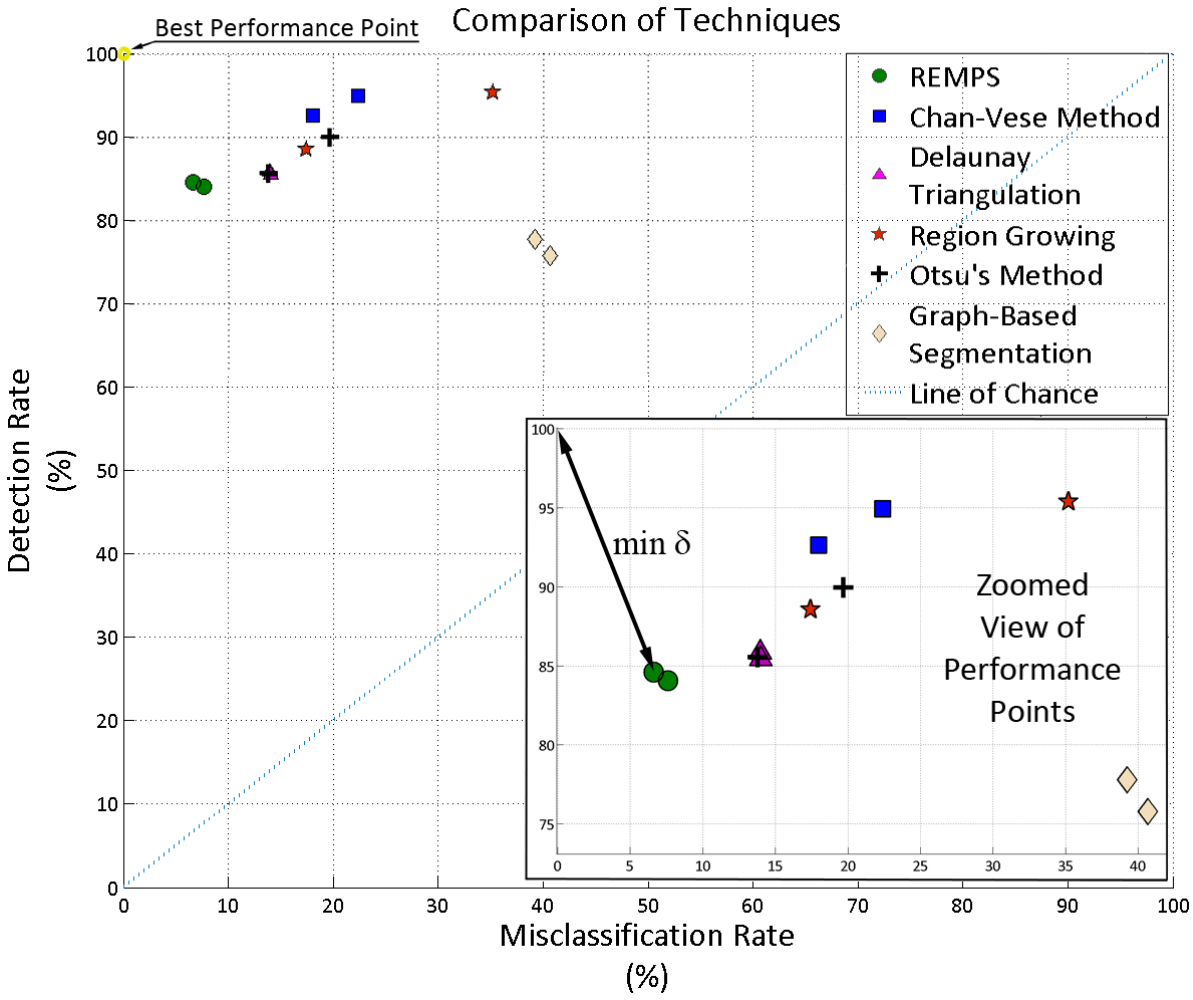

Fig. 9. Comparison of detection techniques through the use of performance points in the ROC space.

REMPS was also applied to a standard image in a non-structural scene, significantly disparate from the corroded example presented in this paper, to showcase its flexibility. A visual comparison with some of the detection techniques previously mentioned is presented in Figure 10, which further illustrates the potential of REMPS and underlines its credentials as a high performing standalone technique beyond damage identification applications.

[Figure 10 here]

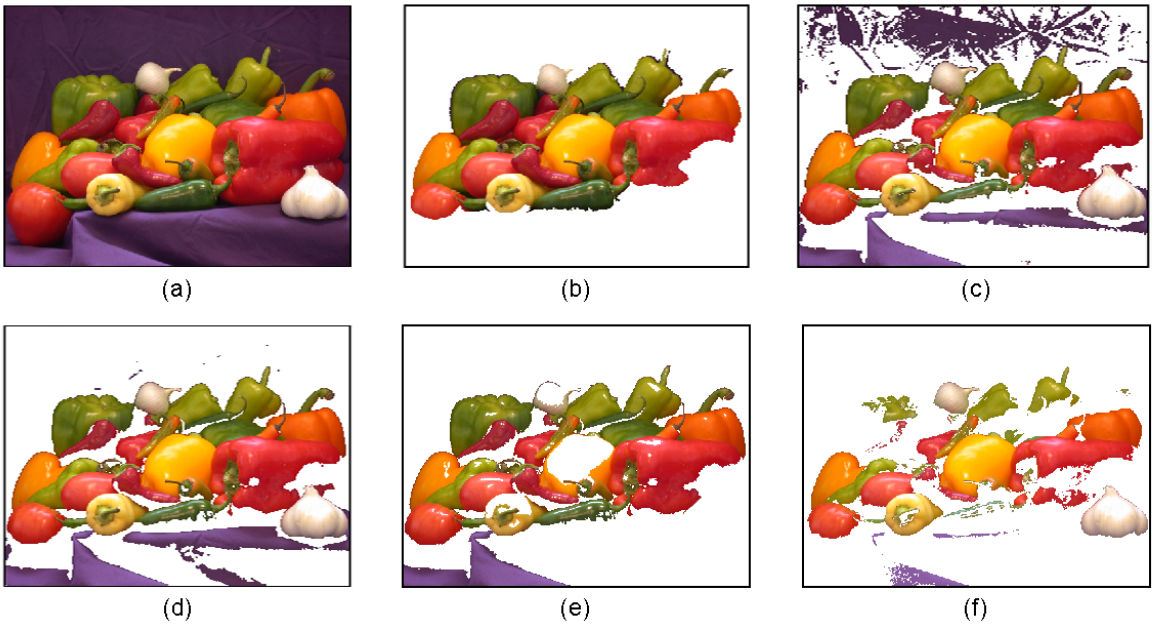

Fig. 10. (a) Original Image, Detected Regions from: (b) REMPS, (c) Chan-Vese Method, (d) Delaunay Triangulation, (e) Region Growing, and (f) Otsu's Method.

It may be observed from Figure 8 and Figure 10 that the detected regions from REMPS produce a much 'cleaner' image of detected regions that is not contaminated by speckles of spurious regions which is a feature of all the other techniques. Having a 'cleaner' image is important for many post-processing applications such as calculating the propagation rate for damaged regions. For such an application, labelling and numbering of damaged regions may be a necessary prerequisite which would be inhibited by the presence of the many small and insignificant spurious regions.

3.4 Comparison with a Texture Analysis Based Technique for Damage Detection

Image processing based techniques include colour intensity based methods and texture analysis based methods. Naturally, the techniques in each group are suited to different applications, depending largely on whether the damaged regions are more separable from the background based on colour or on texture. This section assesses the performance of REMPS alongside a texture analysis based technique (O'Byrne et al, 2013) previously proposed in the domain of NDT, in order to give an indication of the performance levels that can be expected when a range of damage forms and surfaces

are under consideration. This should enable the end user to better decide on which approach is most appropriate to for their needs.

Both methods are applied to four different images shown which feature various damage forms, lighting conditions, viewing angles, resolutions etc. These images are shown in Figure 9, along with the regions detected using REMPS and texture analysis approach.

[Figure 11 here]

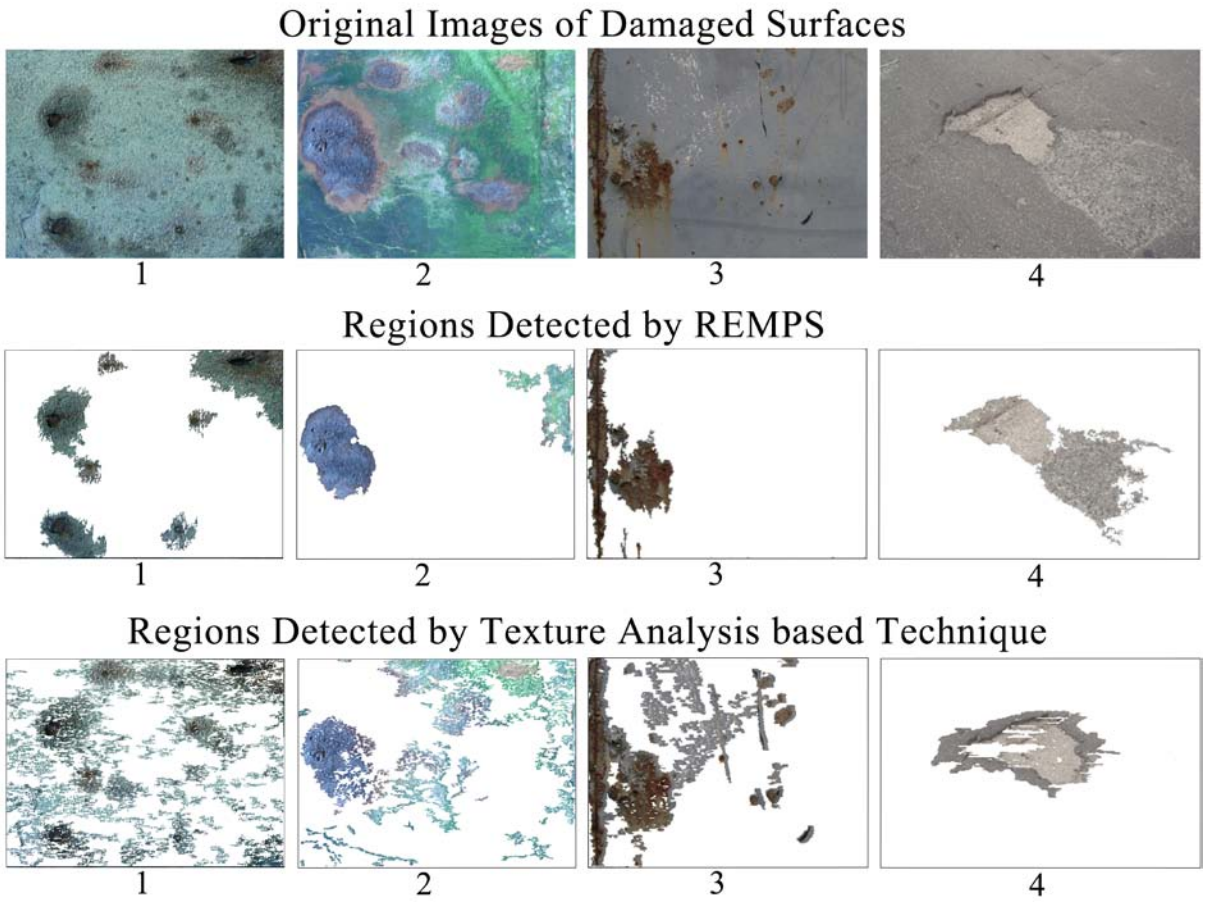

Fig. 11. Top Row: Original Images Featuring Damage: (1) Pitting Corrosion, (2) Marine Growth, (2) Corroded Metal, and (4) Exposed Deck. **Middle Row:** Regions Detected using REMPS. **Bottom Row:** Regions Detected using Texture Analysis.

As with the main illustrated example presented in this paper, the performance of REMPS and the Texture Analysis technique was measured by firstly visually segmenting each of these images based on expert opinion. The visually segmented image was then compared with the detected regions outputted from each technique. The *DR*, *MCR* and corresponding δ were calculated as per the process outlined in Section 2.3. These values are summarized in Table 3.

Table 3

Comparison of REMPS Technique and a Texture Analysis Technique.

Sample Image	REMPS			Texture Analysis		
	DR	MCR	δ	DR	MCR	δ
(1) Pitting Corrosion	84%	8%	0.18	78%	32%	0.39
(2) Marine Growth	64%	8%	0.37	64%	29%	0.46
(3) Corroded Metal	90%	3%	0.11	96%	24%	0.24
(4) Exposed Deck	93%	10%	0.12	52%	10%	0.49

It may be noted from these results that REMPS was quite successful for the majority of cases with the exception of the marine growth image. The poorer detection results for this image may be explained by the fact that the damaged regions throughout the image were not characterized by one single colour. Instead they took on numerous contrasting shades which often overlapped with the non-damaged background. Generally however, REMPS proved effective at locating the presence of damage as well as accurately defining the shape and size of damaged regions.

The texture based method was effective at locating the presence of damage as may be observed from Figure 11, however it did not perform as well as REMPS at defining the extent of damage which resulted in poor *DR*, *MCR* and δ values in Table 3. Many small spurious regions were detected unlike REMPS which produced a 'cleaner' and more homogenous detection.

These results demonstrate the applicability of REMPS for a wide range of damage forms, and show that it offers an improvement over the texture analysis based damage detection approach for the presented scenarios.

4.0 CONCLUSION

Various forms of NDT techniques have been employed to assess civil infrastructure since the advent of SHM, however it is only with the relatively recent introduction of computer based systems that quantitative information on the health status of structural components can be obtained on-site. There

is thus an emphasis on devising sophisticated damage detection techniques that can effectively capitalise on the ever increasing level of computational efficiency. Image based approaches offer an efficient way of acquiring information on the presence and extent of visible damages on the surface of infrastructural elements. As the image acquisition can be carried out by personnel with minimal training, this approach removes the need for expertise at all stages of the inspection process. This paper has presented an image analysis based damage detection technique, REMPS, which is intended to supplement and strengthen existing visual inspection methods by providing a quick and convenient source of quantitative information. The development of REMPS was necessitated by a lack of sophisticated image based damage detection techniques that can be applied to a broad range of surface types, damage forms, and lighting conditions that are typically encountered in infrastructures. The specific application presented in this paper demonstrates the immediate success of the method as an NDT tool to assist visual inspections where an improved detection directly influences the owner of infrastructure systems during a decision-making process.

REMPS adopts a multi-phase segmentation methodology which incorporates features from three standard image processing and data analysis techniques. Since these techniques are well-known and described in the literature, REMPS may be easily replicated and implemented. A key benefit of REMPS is its ability to produce better defined and more homogenous regions of interest without being affected by isolated extraneous pixels. REMPS achieves this cleaner segmentation by efficiently integrating pixel and spatial relationships. The $\alpha\delta$ method was used to measure performance. The presented results indicate that improvements can be made to the detection accuracy by segmenting in the *L*a*b** colour space and adopting a HDR protocol. Furthermore, the credentials of REMPS as a standalone segmentation technique are underlined as it is shown that REMPS outperforms several established detection techniques for various scenes.

ACKNOWLEDGEMENTS

The authors wish to thank the Irish Research Council for Science, Engineering and Technology (IRCSET) for providing grant to support this research and CAPACITES/IXEAD society for the practical assistance.

REFERENCES

Abdel-Qader, I., Yohali, S., Abudayyeh, O. & Yehia, S. (2008), Segmentation of thermal images for non-destructive evaluation of bridge decks, *NDT and E International*, **41**(5), 395-405.

Abdou, I.E., & Pratt, W. (1979), Quantitative design and evaluation of enhancement/thresholding edge detectors, *Proceedings of the IEEE* , **67**(5), 753-763.

Adams, R. & Bischof, L. (1994), Seeded region growing, *Pattern Analysis and Machine Intelligence, IEEE Transactions on*, **16**(6), 641-647.

Agin, G. J. (1980), Computer vision systems for industrial inspection and assembly, *Computer* **13**(5), 11-20.

Alaknanda, R. S. Anand, & Kumar P. (2009), Flaw detection in radiographic weldment images using morphological watershed segmentation technique, *NDT and E International*, **42**(1), 2-8.

Baroth, J., Breysse, D. & Schoefs, F. (2011), Construction Reliability. Wiley, Hoboken, NJ.

Boser, B. E., Guyon, I. M. & Vapnik V.N. (1992), A training algorithm for optimal margin classifiers, *Proceedings of the fifth annual workshop on Computational learning theory*, Pittsburgh, Pennsylvania, United States, ACM**,** 144-152.

Butcher, J. B., Day, C. R., Austin, J. C., Haycock, P. W., Verstraeten, D. & Schrauwen, B. (2013), Defect Detection in Reinforced Concrete Using Random Neural Architectures, *Computer-Aided Civil and Infrastructure Engineering*, In Press.

Chan, T. F. & Vese L.A. (2001), Active contours without edges, *IEEE Transactions on Image Processing*, **10**(2), 266-277.

Cheddad, A., Mohamad, D. & Manaf, A.A. (2008), Exploiting Voronoi diagram properties in face segmentation and feature extraction, *Pattern Recognition*, **41**(12), 3842-3859.

Chi, S., & Caldas, C.H. (2011), Automated Object Identification using Optical Video Cameras on Construction Sites, *Computer-Aided Civil and Infrastructure Engineering*, **26**(5), 368-380.

Cord, A., & Chambon S. (2012), Automatic Road Defect Detection by Textural Pattern Recognition based on AdaBoost, *Computer-Aided Civil and Infrastructure Engineering*, **27**(4), 244-259.

Correa, S., Souza, E., Oliveira, D., Silva, A., Lopes, R., Marinho, C. & Camerini, C. (2009). Assessment of weld thickness loss in offshore pipelines using computed radiography and computational modeling. *Applied Radiation and Isotopes*, **67**(10), 1824-1828.

Cortes, C. & Vapnik, V. (1995), Support-vector networks, *Machine Learning*, **20**(3), 273-297.

Cristianini, N. & Shawe-Taylor, J. (2000), An Introduction to Support Vector Machines and other Kernel-based Learning Methods, Cambridge University Press, Cambridge.

D'Orazio, T., Leo, M., Distante, A., Guaragnella, C., Pianese, V. & Cavaccini, G. (2008), Automatic ultrasonic inspection for internal defect detection in composite materials, *NDT and E International*, **41**(2), 145-154.

Debevec, P.E. & Malik, J. (2008), Recovering high dynamic range radiance maps from photographs. *ACM SIGGRAPH 2008 classes*, Los Angeles, California, ACM, 1-10.

Estes, A.C. & Frangopol, D.M. (2003), Updating bridge reliability based on bridge management systems visual inspection results, *Journal Of Bridge Engineering*, **8**(6) Special Issue, 374-382

Felzenszwalb, P.F. & Huttenlocher, D.P. (2004), Efficient graph-based image segmentation, *International Journal of Computer Vision*, **59**(2), 167-181.

Ghosh, B., Pakrashi, V. & Schoefs, F. (2010), High dynamic range image processing for non-destructive-testing, *European Journal of Environmental and Civil Engineering*, **15**(7), 1085-1096.

Giralt, J., Rodrigez-Benitez, L., Moreno-Garcia, J., Solana-Cipres, C. and L. Jimenez, L. (2013), Lane Mark Segmentation and Identification using Statistical Criteria on Compressed, *Integrated Computer-Aided Engineering*, **20**(2), 143-155.

Groves, D. & Connell, D. (1985). Offshore structure fabrication experience with magnetic particle inspection. *NDT international*, **18**(2), 85-88.

Heriansyah, R. & Abu-Bakar S.A.R. (2009), Defect detection in thermal image for nondestructive evaluation of petrochemical equipments, *NDT and E International*, **42**(8), 729-740.

Hui, Z., Fritts, J.E. & Goldman, S.A. (2008), Image segmentation evaluation: a survey of unsupervised methods, *Computer Vision and Image Understanding*, **110**(2), 260-280.

Iyer, S., & Sinha, S.K. (2006), Segmentation of Pipe Images for Crack Detection in Buried Sewers, *Computer-Aided Civil and Infrastructure Engineering*, **21**(6), 395-410.

Iyer, S. R., Sinha, S. K. & Schokker, A. J. (2005), Ultrasonic C-Scan imaging of post-tensioned concrete bridge structures for detection of corrosion and voids, *Computer-Aided Civil and Infrastructure Engineering*, **20**(2), 79–94.

Kasban H, Zahran, O., Arafa, H., El-Kordy, M., Elaraby, S.M.S. & Abd El-Samie, F.E. (2011), Welding defect detection from radiography images with a cepstral approach, *NDT and E International*, **44**(2), 226-231.

Komorowski, J.P. & Forsyth, D.S. (2000), Role of enhanced visual inspections in the new strategy for corrosion management, *Aircraft Engineering and Aerospace Technology*, **72**(1), 5-13.

Li, D., Xu, L., Goodman, E., Xu, Y. & Wu, Y. (2013), Integrating a statistical background-foreground extraction algorithm and SVM classifier for pedestrian detection and tracking, *Integrated Computer-Aided Engineering*, **20**(3), 201-216.

Liu, Z., Genest, M. & Krys, D. (2012), Processing thermography images for pitting corrosion quantification on small diameter ductile iron pipe, *NDT and E International*, **47**, 105-115.

Lu, C.S., Chung, P.C. & Chen, C.F. (1997), Unsupervised texture segmentation via wavelet transform, *Pattern Recognition*, **30**(5), 729-742.

Molero, M., Aparicio, S., Al-Assadi, G., Casati, M.J., Hernández, M.G. & Anaya, J.J. (2012), Evaluation of freeze-thaw damage in concrete by ultrasonic imaging, *NDT and E International*, *In press*.

Naccari, F., Battiato, S., Bruna, A., Capra, A., & Castorina, A. (2005), Natural scenes classification for color enhancement, *Consumer Electronics, IEEE Transactions on*, **51**(1), 234-239.

Nishikawa, T., Yoshida, J., Sugiyama T., & Fujino, Y. (2012), Concrete Crack Detection by Multiple Sequential Image Filtering, *Computer-Aided Civil and Infrastructure Engineering*, **27**(1), 29-47.

Nugent, M. J. & Pellegrino, B. A. (1991), Remote visual testing (RVT) for the diagnostic inspection of feedwater heaters. *in Proceedings of the 1991 International Joint Power Generation Conference*, October 6, 1991— October 10, 1991, American Society of Mechanical Engineers (ASME), Nuclear Engineering Division (Publication), pp. 55–62.

O'Byrne, M., Ghosh, B., Pakrashi, V. & Schoefs, F. (2013), Effects of turbidity and lighting on the performance of an image processing based damage detection technique, *11th International Conference on Structural Safety & Reliability*, Columbia University, New York, NY.

O'Byrne, M., Pakrashi, V., Ghosh, B. & Schoefs, F. (2011), Receiver operating characteristics of a modified edge detection for corrosion classification. *Forum Bauinformatik 23rd European Conference*, Cork, Ireland.

O'Byrne, M., Schoefs, F., Pakrashi, V. & Ghosh, B. (2013), Texture Analysis Based Damage Detection of Ageing Infrastructural Elements, *Computer-Aided Civil and Infrastructure Engineering*, **28**(3), 162-177.

O'Gorman, L., Sammon, M.J. & Seul, M. (2008), *Practical algorithms for image analysis*, Cambridge University Press, New York.

Osornio-Rios, R. A., Amezquita-Sanchez, J. P., Romero-Troncoso, R. J. & Garcia-Perez, A. (2012), MUSIC-ANN Analysis for Locating Structural Damages in a Truss-Type Structure by Means of Vibrations, *Computer-Aided Civil and Infrastructure Engineering*, **27**(9), 687-698.

Otsu, N. (1979), Threshold selection method from gray-level histograms, *IEEE Transactions on Systems, Man and Cybernetics*, **9**(1), 62-66.

Park, H.S., H.M. Lee, H.M., Adeli, H. & Lee, I. (2007), A New Approach for Health Monitoring of Structures: Terrestrial Laser Scanning, *Computer-Aided Civil and Infrastructure Engineering*, **22**(1), 19-30.

Pakrashi, V., Schoefs, F., Memet, J.B. & O'Connor, A. (2010), ROC dependent event isolation method for image processing based assessment of corroded harbour structures, *Structure and Infrastructure Engineering: Maintenance, Management, Life-Cycle Design and performance (NSIE)*, **6**(3), 365-378.

Peska, B. (2001), Applications of laser-based nondestructive testing (NDT) for tube / pipe inspection, *2001 ASME Pressure Vessels and Piping Conference*, July 23, 2001 - July 26, 2001, Atlanta, GA, United states, American Society of Mechanical Engineers.

Phares, B., Washer, G., Rolander, D., Graybeal, B. & Moore, M. (2004), Routine Highway Bridge Inspection Condition Documentation Accuracy and Reliability, *Journal of Bridge Engineering*, 9(4), 403-413.

Pizer, S.M., Amburn, E.P., Austin, J.D., Cromartie, R., Geselowitz, A., Greer, T., ter Haar Romeny, B., Zimmerman, J.B. & Zuiderveld, K. (1987), Adaptive histogram equalization and its variations, *Computer Vision, Graphics, and Image Processing*, **39**(3), 355-368.

Reinhard, E., Khan, E.A., Akyz, A.O. & Johnson G.M. (2008), Color Imaging: Fundamentals and Applications, Natick, MA, USA.

Rouhan, A. & Schoefs, F. (2003), Probabilistic modeling of inspection results for offshore structures, *Structural Safety*, **25**(4), 379-399.

Sarma, K.C. & Adeli, H. (1998), Cost optimization of concrete structures, *Journal of Structural Engineering*, **124**(5), 570-578.

Schoefs F., Bernard O., Capra B., & Aduriz X. (2009), Comparison of additional costs for several replacement strategies of randomly ageing reinforced concrete pipes, *Computer Aided Civil and Infrastructure Engineering*, **24**(7), 492-508

Schoefs, F., Abraham, O., & Popovics, J. (2012a), Quantitative evaluation of NDT method performance: application example based on contactless impact echo measurements for void detection in tendon duct, *Construction and Building Materials (CBM), In Press*.

Schoefs, F., Clément, B.J. & Capra, B.A. (2012b.), The αδ method for modelling expert Judgment and combination of NDT tools in RBI context: application to Marine Structures, Structure and Infrastructure Engineering: Maintenance, Management, Life-Cycle Design and performance (NSIE), *Monitoring, Modeling and Assessment of Structural Deterioration in Marine Environments*, **8**(Special Issue), 531-543.

Sinha, S.K., Fieguth, P.W., & Polak, M.A. (2003). Computer Vision Techniques for Automatic Structural Assessment of Underground Pipes, *Computer-Aided Civil and Infrastructure Engineering*, **18**(2), 95-112.

Sinha, S.K., & Fieguth, P.W. (2006). Automated detection of cracks in buried concrete pipe images, *Automation in Construction*, **15**(1), 58-72.

Sirca Jr, G.F. & Adeli, H. (2005), Cost optimization of prestressed concrete bridges, *Journal of Structural Engineering*, **131**(3), 380-388.

Sohn, H., Kim, S. D. & Harries, K. (2008), Reference-free damage classification based on cluster analysis, *Computer-Aided Civil and Infrastructure Engineering*, **23**(5), 324–38.

Song, M., & Civco, D. (2004), Road extraction using SVM and image segmentation, *Photogrammetric Engineering and Remote Sensing*, **70**(12), 1365-1371.

Vapnik, V. N. (1995), *The Nature of Statistical Learning Theory*. Springer-Verlag, New York.

Vilar, R., Zapata, J. & Ruiz, R. (2009), An automatic system of classification of weld defects in radiographic images, *NDT and E International*, **42**(5), 467-476.

Yazid, H., Arof, H., Yazid, H., Ahmad, S., Mohamed, A.A. & Ahmad F. (2011), Discontinuities detection in welded joints based on inverse surface thresholding, *NDT and E International*, **44**(7), 563-570.

Yishuo, H., & Jer-Wei, W. (2010), Infrared thermal image segmentations employing the multilayer level set method for non-destructive evaluation of layered structures, *NDT and E International*, **43**(1), 34-44.

Yusa, N., Janousek, L., Rebican, M., Chen, Z., Miya, K., Chigusa, N. & Ito, H. (2006), Detection of embedded fatigue cracks in Inconel weld overlay and the evaluation of the minimum thickness of the weld overlay using eddy current testing, *Nuclear Engineering and Design*, **236**(18), 1852–59.